Finite Reynolds number effect and the 4/5 law

R. A. Antonia,[1,2] S. L. Tang,[1,3,*] L. Djenidi,[2] and Y. Zhou[1,3]

[1]*Institute for Turbulence-Noise-Vibration Interaction and Control, Harbin Institute of Technology, Shenzhen 518055, People's Republic of China*
[2]*School of Engineering, University of Newcastle, Callaghan, New South Wales 2308, Australia*
[3]*Digital Engineering Laboratory of Offshore Equipment, Shenzhen 518055, People's Republic of China*

Kolmogorov [A. N. Kolmogorov, Dokl. Akad. Nauk SSSR **30**, 299 (1941)] formulated a theory of small-scale turbulence (K41), valid at extremely large Reynolds numbers, based on two similarity hypotheses and on an exact result derived from the transport equation for the second-order structure function, known as the 4/5 law. Although K41 was praised for its simplicity and elegance, Kolmogorov [A. N. Kolmogorov, J. Fluid Mech. **13**, 82 (1962).] proposed a new refined similarity hypothesis (K62) mainly to account for the effect of the large scales on the small scales. It has been widely interpreted in the literature as a correction to K41 arising from the intermittency of the instantaneous energy dissipation rate ϵ. In this paper we argue that since K62 retains the 4/5 law, it must satisfy the same constraints as K41, viz., extremely large Reynolds number and flow stationarity. The retention of the 4/5 law is not however consistent with the presence of nonstationarity due to the effect of the large scales, as postulated by K62. A relatively extensive survey of published data shows that, indeed, the 4/5 law has not yet been observed in either experiments or simulations due to the Reynolds number not being sufficiently large. The use of the transport equation for the second-order structure function, together with an empirical model for the Kolmogorov-normalized second-order velocity structure function, confirms that the 4/5 law is established only after this structure function becomes independent of the Reynolds number.

I. INTRODUCTION

Kolmogorov's 1941 theory (K41) [1,2], which requires the Reynolds number to be infinitely large, is based on two similarity hypotheses. The first (H1) states that, for locally isotropic turbulence, the statistical properties associated with the small scales are uniquely determined by the kinematic viscosity ν and the mean turbulent kinetic dissipation rate $\overline{\epsilon}$ (the overbar represents time and/or spatial average). Using H1, Kolmogorov deduced, from dimensional analysis, a length scale $\eta = (\nu^3/\overline{\epsilon})^{1/4}$ and a velocity scale $v_K = (\nu\overline{\epsilon})^{1/4}$ (η is the scale at which energy is dissipated through the viscosity). The second hypothesis (H2), again for locally isotropic turbulence, states that over a range of scales much larger than η but much smaller than the integral scale L (loosely identified as the scale at which turbulent energy is introduced) the statistical properties of turbulence are uniquely determined by $\overline{\epsilon}$ and do not depend on ν. Using H1 and H2, Kolmogorov [1] derived the two-thirds law, i.e.,

$$\overline{(\delta u)^2} = C_2 \overline{\epsilon}^{2/3} r^{2/3}, \tag{1}$$

*shunlin.tang88@gmail.com

where δu [$=u(x + r, t) - u(x, t)$] is the velocity increment, r is the spatial increment, and C_2 is a universal constant. However, in the same year, he used the von Kármán–Howarth equation [3]

$$-\overline{(\delta u)^3} = \frac{4}{5}\bar{\epsilon}r - 6\nu\frac{\partial\overline{(\delta u)^2}}{\partial r} + \underbrace{\frac{3}{r^4}\int_0^r s^4\frac{\partial\overline{(\delta u)^2}}{\partial t}ds}_{I_u},$$ (2)

where s is a dummy index of integration, to derive the 4/5 law for homogeneous and isotropic turbulence (HIT), viz.,

$$-\overline{(\delta u)^3} = \frac{4}{5}\bar{\epsilon}r,$$ (3)

where r lies in the inertial range (IR) $\eta \ll r \ll L$. The relation (3) follows from (2) provided both the viscous term and the nonstationary term (here denoted by I_u), which in essence represents the effect of the large scales, can be neglected. Kolmogorov justified the removal of these terms by requiring the Reynolds number to be very large. There is little doubt that Eq. (3) is pivotal for any asymptotic theory of small-scale turbulence; a measure of its importance in turbulence research is reflected in the number of times it is cited across different chapters dedicated to prominent turbulence researchers in Ref. [4]. K41 was introduced to western researchers by Batchelor [5], who scrutinized all aspects of K41, including the derivation of (3), and received promising experimental support, in the context of the spectrum of u, some 20 years after it was first published [6]. However, mainly in response to a remark by Landau, Kolmogorov [7] felt compelled to revise his original theory by introducing a refined similarity hypothesis, purportedly to account for the variation in $\bar{\epsilon}$ induced by the large (external) scales. He assumed a log-normal model, as obtained by Oboukhov [8], for ϵ_r, the subscript denoting averaging over a sphere of diameter r. The variable $\delta u/(r\bar{\epsilon})^{1/3}$ in K41 was now replaced by $\delta u/(r\epsilon_r)^{1/3}$. It should be noted that the log-normal model was proposed for the IR but subsequently extended to the dissipative range by other researchers (e.g., [9–11]) and replaced by a plethora of other types of intermittency models [12–17]. According to Saffman [18], the physical basis of K41, i.e., the hypothesis of a cascade of energy from large to small scales, is supposedly invalidated by the spatial intermittency of the dissipative process, so new results now depend on the intermittency model that is used. Indeed, the physics, and hence the consequences for the small-scale statistics, was completely changed. We have recently reexamined the behavior of dissipative range quantities such as the skewness and flatness factor of $\partial u/\partial x$, the longitudinal velocity derivative, in various turbulent flows and found that the behavior of these quantities, as Re_λ [$=u'\lambda/\nu$, where λ is the longitudinal Taylor microscale $u'/(\partial u/\partial x)'$ and a prime denotes a rms value] increases, is more aligned with K41 than with K62. In this paper we focus on the IR behavior of $\overline{(\delta u)^n}$ for $n = 2$ and 3.

K41 predicts

$$\overline{(\delta u^*)^n} = C_{un}r^{*n/3},$$ (4)

where the asterisk superscript denotes normalization by η, and v_K and C_{un} are the Kolmogorov universal constants. In particular, $C_{u3} = -4/5$ since Eq. (3) can be rewritten as

$$-\overline{(\delta u^*)^3} = \frac{4}{5}r^*.$$ (5)

Apart from C_{u3}, the other constants in (4) are not known theoretically.

On the other hand, K62 predicts that

$$\overline{|\delta u|^n} = D_{un}(x, t)(\bar{\epsilon}r)^{n/3}\left(\frac{L}{r}\right)^{\mu n(n-3)/18},$$ (6)

where D_{un} are constants which depend on the macrostructure of the flow and are functions of the spatial location x and t. The L is usually identified as the integral scale (Kolmogorov refers to L as the external scale) and μ (or k in Kolmogorov's 1962 paper) is commonly referred to as the

intermittency exponent (sometimes intermittency correction), assumed to be universal (with a value of about 0.2). We now have a scenario where the external (large) scales can affect the IR so that both the Kolmogorov constants (K41) and the exponent of r are modified. The notable exemption is $\overline{(\delta u)^3}$, which is assumed in K62 to be given by (3). The deviation of the exponent from $n/3$ has been seemingly confirmed by data from experiments and direct numerical simulations. It has also been emulated by many intermittency models. As a result, the generally accepted behavior of $\overline{(\delta u)^n}$ in the IR is

$$\overline{(\delta u)^n} \sim r^{\zeta_n}, \tag{7}$$

where $\zeta_n > n/3$ for $n < 3$ and $\zeta_n < n/3$ for $n > 3$. The distribution of ζ_n vs n is convex, in contrast to the linear variation [relation (4)] of K41. Despite the shortcomings of the log-normal model, Eq. (6) seems to represent the variation of ζ_n with n reasonably well, at least for $n \leqslant 8$.

At this stage, there are two major comments that need to be made. First, it should be fully recognized that K41 and K62 are asymptotic theories, valid strictly at very large Re_λ. In particular, the derivation of Eq. (3) requires the second and third terms on the right-hand side of Eq. (2) to be negligible. The term I_u hinders the establishment of a credible IR since it is the dominant term as r continues to increase [when r exceeds L, I_u and the first term on the right-hand side of (2) represent the conventional overall energy budget]. It is difficult to see how (3) can be derived unless I_u disappears; yet, K62 asserts that K41 needs to be modified due to the effect from the external scales. McComb [19] correctly points out that there is an inconsistency between the left- and right-hand sides of Eq. (6) since the left-hand side should depend only on r in HIT. He also states that the 4/5 law "emerges unscathed" from K62. This is not evident since the 4/5 law is simply assumed in K62 in order to provide an expression for the skewness of δu in the IR. Using the framework of K62, Eq. (3) can be recast as

$$-\frac{\overline{(\delta u)^3}}{u'^3} = \frac{4}{5} C_\epsilon \frac{r}{L} \tag{8}$$

after replacing $\overline{\epsilon}$ by $C_\epsilon u'^3/L$, where C_ϵ is the dimensionless energy dissipation coefficient. The 4/5 law survives only if $C_\epsilon = 1$; the available data [20–24] indicate that the magnitude of C_ϵ depends on the flow (it is unlikely that C_ϵ is exactly 1). There is no doubt that K62 preserves the value of 1 for the exponent of r, as do all post-K62 intermittency models.

For $n = 2$, Eq. (6) yields

$$\overline{(\delta u)^2} \sim (\overline{\epsilon} r)^{2/3} \left(\frac{L}{r}\right)^{-\mu/9}. \tag{9}$$

Since Kolmogorov's equation, i.e., Eq. (2) with $I_u = 0$, satisfies similarity when normalized by v_K and η (see, e.g., [5,25]), we are entitled to normalize (9) using v_K and η. This leads to

$$\overline{(\delta u^*)^2} \sim r^{*2/3+\mu/9} \mathrm{Re}_\lambda^{-8\mu/6}. \tag{10}$$

Since $\mu > 0$, $\overline{(\delta u^*)^2}$ will decrease to zero as $\mathrm{Re}_\lambda \to \infty$. This trend, which is inconsistent with that obtained by Oboukhov [8], does not seem realistic, nor can it be reconciled with the way estimates of C_{u2} have been made in the literature, either directly using Eq. (4) (e.g., [26]) or via the spectrum of u (e.g., [27]). These estimates should have varied with Re_λ systematically if Eq. (10) were valid. Given the close link that exists between $\overline{(\delta u)^2}$ and $\overline{(\delta u)^3}$ through Eq. (2), it seems unlikely that $\overline{(\delta u^*)^2}$ will continue to depend on the Reynolds number after $\overline{(\delta u^*)^3}$ $(=-4/5r^*)$ becomes independent of Re_λ. All of the previously mentioned inconsistencies lead us to question the inclusion of L in Eq. (6), which is the major idea on which K62 is founded.

Second, it should be recognized that measurements and numerical simulations are carried out at finite Reynolds numbers and there is no guarantee that ζ_n [Eq. (7)] can be estimated without ambiguity. In their review of small-scale turbulence, Sreenivasan and Antonia [13] noted

that although the experimental support for the anomalous scaling was overwhelming, several uncertainties remained, in particular the need to account for the finite Reynolds number (FRN) effect, "which is not understood and cannot be calculated *a priori*," and the practical issue of "how one defines the scaling range and obtains scaling exponents from [power laws] of modest quality." Since that review, several papers have dwelt on the FRN effect starting either with Eq. (2) in physical space or von Kármán and Lin's equation [28] in spectral space, i.e., without neglecting the nonstationarity and without introducing any arbitrary intermittency model [19,29–37]. This approach is solidly underpinned by the fact that the von Kármán–Howarth equation is valid at any Reynolds number. This has been exploited successfully by experimentalists (see, e.g., [38,39]) to calculate the triple-velocity correlation [or $\overline{(\delta u)^3}$] starting with the measured double-velocity correlation [or $\overline{(\delta u)^2}$]. It also accounts for intermittency in a natural manner since intermittency, an unmistakable characteristic of turbulence, is intrinsically embedded in the transport equation for $\overline{(\delta u)^2}$. The use of this approach has certainly heightened the need to increase Re_λ as much as possible in the quest for establishing an IR. Interestingly, experiments and numerical simulations [40–44] have provided strong support for many consequences of H1 (K41) at small to moderate values of the Reynolds number ($Re_\lambda \lesssim 1000$). This is not surprising since it has been shown that Eq. (2) admits similarity at small scales (over a range of r in which $I_u \approx 0$) based on η and v_K (see, e.g., [25,45]) even at modest values of Re_λ; the range of validity of this scale invariance extends as Re_λ increases. Supporters of K62 argue that the anomalous scaling is real and that the best way of highlighting it is to focus on large values of n (since the difference between ζ_n and $n/3$ is small for $n \leqslant 4$). This argument can be countered, if not dismissed, on the basis that the larger n is, the greater the value of Re_λ that is required to ensure independence of $\overline{(\delta u^*)^n}$ (in the IR) from the Reynolds number. Tang *et al.* [44] provide some experimental evidence for this trend, even though the maximum value of Re_λ is insufficient. More importantly, if ζ_2 and ζ_3 cannot be estimated rigorously, why should one trust the data for ζ_n ($n \geqslant 4$), especially in view of the continuous evolution with Re_λ of $\overline{(\delta u^*)^n}$ in what is loosely described as the scaling range [44]; this evolution is more accentuated as n increases. The arguments presented in this and previous paragraphs lead us to believe that it is important, if not crucial, to first ascertain the evolution with Re_λ of $\overline{(\delta u)^2}$ and $\overline{(\delta u)^3}$, in the context of Eq. (2), in flows where external scales can, through I_u, affect the establishment of the IR differently.

In Secs. II and III we present a relatively extensive review of experimental and numerical data for $\overline{(\delta u)^2}$ and $\overline{(\delta u)^3}$, as reported in the literature, with the aim of assessing the behavior of these quantities as Re_λ increases. In order to extrapolate the behavior of $\overline{(\delta u)^3}$ when $Re_\lambda \to \infty$, we use, like Antonia and Burattini [34], an empirical model for $\overline{(\delta u)^2}$; justification for this approach is provided by comparing measured distributions of $\overline{(\delta u)^3}$ with those inferred from the model using Eq. (2). The conclusions from this review and the model-based extrapolation to $Re_\lambda \to \infty$ are presented in Sec. IV.

II. RESULTS FOR $\overline{(\delta u)^3}$

We report in Fig. 1 a selection of distributions of $-\overline{(\delta u^*)^3}/r^*$ based on published data. The selection is not exhaustive as we have restricted our attention to flows often encountered in the literature: shearless and sheared grid turbulence, along the axes in the far field of plane and circular jets, stationary forced periodic box turbulence (SFPBT), the flow in a cylindrical container between counterrotating end disks, and a boundary layer at $y/\delta \approx 0.5$ (δ is the boundary thickness). Except for Fig. 1(f), which to conserve space includes two rather disparate flows, the other components of Fig. 1 focus on essentially similar flows. In each case, the effect of the large scales on the small scales is likely to be different since the term I_u in Eq. (2) can differ from flow to flow. Expressions for I_u, which reflects the energy balance at large scales, can be found in Ref. [44]. However, I_u can be estimated with relatively good accuracy in only a few flows: grid turbulence, on the axis of a circular jet, along the centerline of a fully developed channel flow, and in box turbulence.
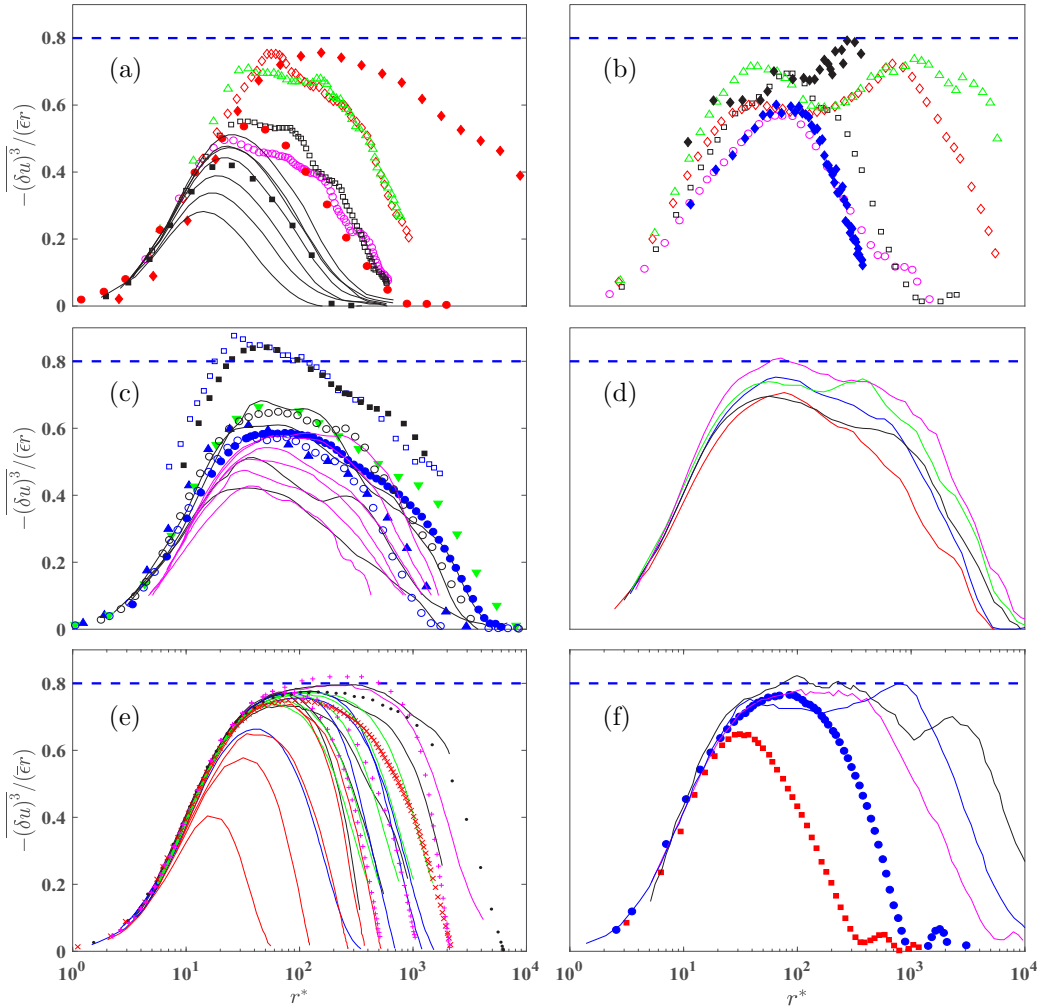
FIG. 1. Distributions of $\overline{(\delta u^*)^3}/r^*$ in various flows. (a) Shearless grid turbulence: black curves, $\mathrm{Re}_\lambda = 26$–99 [40]; ■, $\mathrm{Re}_\lambda = 72$ [46]; ●, $\mathrm{Re}_\lambda = 144$ [46]; ○, $\mathrm{Re}_\lambda = 99$ [47]; □, $\mathrm{Re}_\lambda = 134$ [47]; △, $\mathrm{Re}_\lambda = 319$ [47]; and ◇, $\mathrm{Re}_\lambda = 448$ [47]. Also shown are the data along the axis of the ONERA wind tunnel (similar to grid turbulence) at $\mathrm{Re}_\lambda = 2260$, ◆ [46]. (b) Sheared grid turbulence: ◆, $\mathrm{Re}_\lambda = 170$ [48]; ◆, $\mathrm{Re}_\lambda = 660$ [48]; ○, $\mathrm{Re}_\lambda = 196$ [49]; □, $\mathrm{Re}_\lambda = 254$ [49]; ◇, $\mathrm{Re}_\lambda = 875$ [49]; and △, $\mathrm{Re}_\lambda = 938$ [49]. (c) Along the axis of a circular jet: ■, $\mathrm{Re}_\lambda = 835$ [50]; □, $\mathrm{Re}_\lambda = 966$ [51]; black curves, $\mathrm{Re}_\lambda = 235$–$545$ [52]; ●, $\mathrm{Re}_\lambda = 485$ [41]; pink curves, $\mathrm{Re}_\lambda = 122$–$310$ [53]; ▲, $\mathrm{Re}_\lambda = 350$ [46]; ▼, $\mathrm{Re}_\lambda = 695$ [46]; ○, $\mathrm{Re}_\lambda = 200$ [54]; and ○, $\mathrm{Re}_\lambda = 430$ [54]. (d) Along the axis of a plane jet: $\mathrm{Re}_\lambda = 550$–$1067$ [44]. (e) SFPBT: red curves, $\mathrm{Re}_\lambda = 38$–240 [43]; green curves, $\mathrm{Re}_\lambda = 177$–$435$ [36]; blue curves, $\mathrm{Re}_\lambda = 70$–460 [42]; black curves, $\mathrm{Re}_\lambda = 167$–$1131$ [22]; pink curve, $\mathrm{Re}_\lambda = 805$ [55]; •, $\mathrm{Re}_\lambda = 1300$ [56]; ✕, $\mathrm{Re}_\lambda = 650$ [57]; and +, $\mathrm{Re}_\lambda = 240$–$700$ [58]. (f) In a cylindrical container between counterrotating disks (■, $\mathrm{Re}_\lambda = 120$; ●, $\mathrm{Re}_\lambda = 300$; and pink curve, $\mathrm{Re}_\lambda = 1170$) [59] and at $y/\delta \approx 0.5$ in a high Reynolds number boundary layer: $\mathrm{Re}_\lambda = 600$ (blue curve) and $\mathrm{Re}_\lambda = 1450$ (black curve) [26]. The dashed horizontal line in each plot corresponds to the value of 4/5.
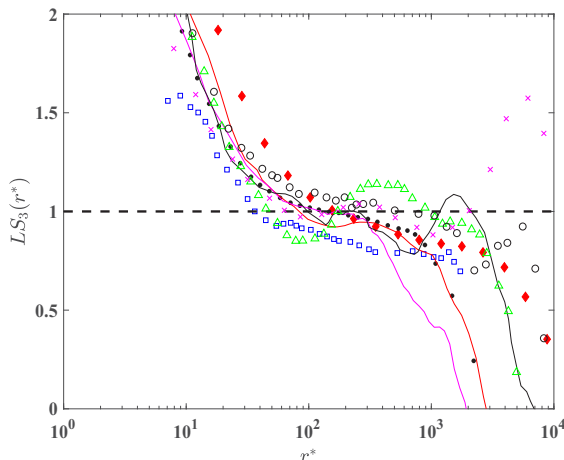
FIG. 2. Local slope $[\mathrm{LS}_3(r^*) = d \log \overline{(\delta u^*)^3}/d \log r^*]$ corresponding to the highest Re_λ in each plot of Fig. 1: ◆, $\mathrm{Re}_\lambda = 2260$ [shearless grid turbulence; see Fig. 1(a)]; △, $\mathrm{Re}_\lambda = 938$ [sheared grid turbulence; see Fig. 1(b)]; □, $\mathrm{Re}_\lambda = 966$ [circular jet; see Fig. 1(c)]; red curve, $\mathrm{Re}_\lambda = 1067$ [plane jet; see Fig. 1(d)]; ●, $\mathrm{Re}_\lambda = 1300$ [SFPBT; see Fig. 1(e)]; black curve, $\mathrm{Re}_\lambda = 1450$ [boundary layer; see Fig. 1(f)]; and pink curve, $\mathrm{Re}_\lambda = 1170$ [flow between counterrotating disks; see Fig. 1(f)]. Also shown are ASL data (○, $\mathrm{Re}_\lambda = 10, 304$ [62]; ×, $\mathrm{Re}_\lambda = 10^4$ [64]). The black dashed line corresponds to the value of 1.

The local slope $\mathrm{LS}_3(r^*) = d[\log \overline{(\delta u^*)^3}]/d[\log(r^*)]$, corresponding to the highest Re_λ in each of the flows considered in Fig. 1 is shown in Fig. 2. Since the atmospheric surface layer (ASL) data are not suitable for testing K41 or K62 because of the likely effects of the mean shear, the strong inhomogeneity of the large scales, and the blockage effect caused by the proximity to a solid boundary [60] (see also [61]), we have not included these data in Fig. 1. We recall, however, that Eq. (3) is not satisfied for the ASL data, as already noted by Sreenivasan and Dhruva [62]; as an example, we show in Fig. 2 one distribution of the ASL data at $\mathrm{Re}_\lambda \sim 10^4$ [62]. Kholmyansky *et al.* [63] pointed out that, for their ASL data at $\mathrm{Re}_\lambda = 10^4$, $-\overline{(\delta u^*)^3}/r^*$ is equal to 0.8 ± 0.05 over at least three decades of r^* [≈ 30–(3.5×10^3)]. However, the estimated local slope $\mathrm{LS}_3(r^*)$ from Fig. 2(a) of Kholmyansky and Tsinober [64] at $\mathrm{Re}_\lambda = 10^4$, which is also shown in Fig. 2, does not have a plateau, implying that Eq. (3) is actually far from being satisfied by their data.

Some remarks are warranted before discussing Figs. 1 and 2. A key element of K41 and K62 is the assumption that the small-scale motion is isotropic. We have shown previously that local isotropy (LI) is satisfied closely in the dissipative range at $r^* \approx 1$ [61,65–68] in the absence of a mean shear. For sheared grid turbulence [Fig. 1(b)], there is a strong departure from LI [69]. As r^* increases to a value that lies within what is loosely identified as the scaling range, LI is satisfied closely in shearless grid turbulence and on the axis of a circular jet (see, e.g., Fig. 4 of [70]). Gotoh *et al.* [42] noted that, for SFPBT, "the isotropy of the [second-] and [third-order] moments (of δu) is excellent for scales less than $L/2$" at $\mathrm{Re}_\lambda = 128$–$460$. However, Tang *et al.* [44] showed that, although the range of r^* in the plane jet ($550 \leqslant \mathrm{Re}_\lambda \leqslant 1067$) which satisfies LI improves as Re_λ increases, the departure from LI remains significant in the scaling range for both $\overline{(\delta u)^2}$ and $\overline{(\delta u)^3}$. There has been no examination of LI in the scaling range for the flow in a cylindrical container between counterrotating end disks. In the boundary layer at $y/\delta \approx 0.5$ ($\mathrm{Re}_\lambda = 600$ and 1450), Saddoughi and Veeravalli's spectral tests indicate that, for wave numbers in the dissipative range, isotropy is adequately satisfied but it is not satisfied in the scaling range. Overall, based on the above discussion, only the shearless grid turbulence, circular jet, and SFPBT satisfy LI to a reasonable degree over both dissipative and scaling ranges for the flows considered in Fig. 1.
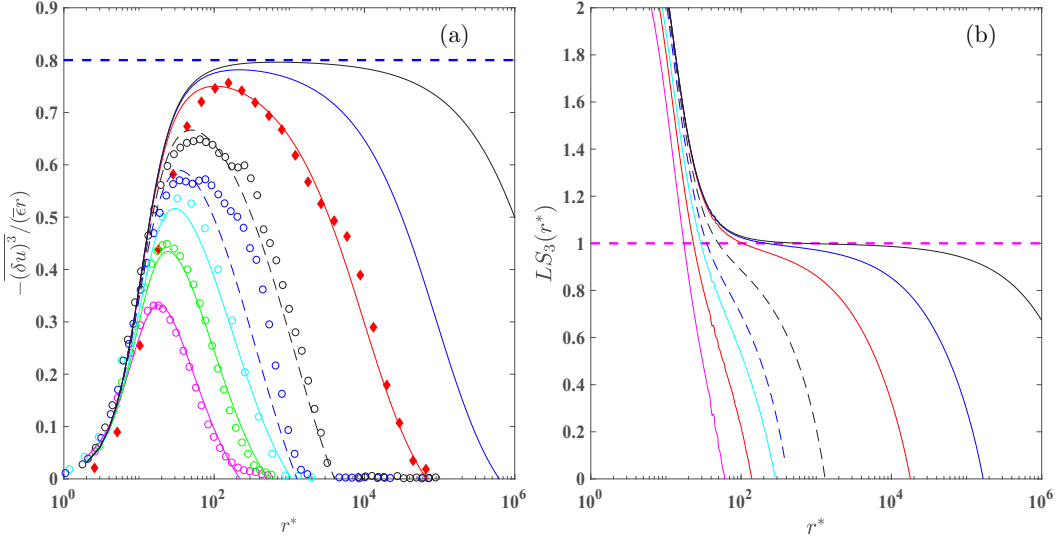
FIG. 3. (a) Analytical predictions of $\overline{(\delta u^*)^3}/r^*$ based on Eqs. (11) and (2) at $Re_\lambda = 51$ (pink curve), $Re_\lambda = 89$ (green curve), $Re_\lambda = 144$ (cyan curve), $Re_\lambda = 2260$ (red curve), $Re_\lambda = 10^4$ (blue solid curve), and $Re_\lambda = 10^5$ (black solid curve). The symbols are the grid turbulence data [see Fig. 1(a)] at $Re_\lambda = 51$ (◯), $Re_\lambda = 89$ (◯), $Re_\lambda = 144$ (◯), and $Re_\lambda = 2260$ (◆). Also shown are the analytical predictions of $\overline{(\delta u^*)^3}/r^*$ based on Eqs. (11) and (13) at $Re_\lambda = 200$ (blue dashed curve) and $Re_\lambda = 430$ (black dashed curve), respectively. The symbols are the circular jet data [see Fig. 1(c)] at $Re_\lambda = 200$ (◯) and $Re_\lambda = 430$ (◯). The dashed horizontal line corresponds to 4/5. (b) Corresponding local slope $[LS_3(r^*) = d \log \overline{(\delta u^*)^3}/d \log r^*]$ at $Re_\lambda = 51$ (pink curve), $Re_\lambda = 89$ (green curve), $Re_\lambda = 144$ (cyan curve), $Re_\lambda = 200$ (blue dashed curve), $Re_\lambda = 430$ (black dashed curve), $Re_\lambda = 2260$ (red curve), $Re_\lambda = 10^4$ (blue solid curve), and $Re_\lambda = 10^5$ (black solid curve). The dashed horizontal line corresponds to the value of 1.

The following comments can be made with regard to Figs. 1 and 2.

(i) None of the distributions in Fig. 1 exhibit a convincing plateau, underlining the absence of an IR [except perhaps for Figs. 1(b) and 4(b), the convex curvature exhibited by the distributions near their peak value persists to the largest value of Re_λ]. This is confirmed by the corresponding behavior of the local slope $[LS_3(r^*) = d \log \overline{(\delta u^*)^3}/d \log r^*]$ of $\overline{(\delta u)^3}$ (Fig. 2), i.e., a power-law behavior for $\overline{(\delta u)^3}$ is strictly untenable. The convex curvature mentioned above complies with Eq. (2) and should be dissociated from experimental uncertainties in $\overline{(\delta u)^2}$ and $\overline{(\delta u)^3}$.

(ii) In Fig. 1(a), only the passive grid data [34,46] display a systematic (and well-behaved) increase with increasing Re_λ. There is much more scatter in the active grid data beyond the maximum value of $-\overline{(\delta u^*)^3}/r^*$ [47]. This behavior is further emphasized in Fig. 1(b) for sheared grid turbulence where the active grid data ($Re_\lambda = 875$ and 938) exhibit two clear peaks, compared to only one peak for the passive grid data. The trend of the Modane (ONERA closed-circuit wind tunnel) data ($Re_\lambda = 2260$) in Fig. 1(a), which are closest to reaching the value of 4/5 with a flattening off around the peak, suggests that Re_λ still needs to be significantly larger before an IR is established. This supports the conclusions reached by Qian [29] and Antonia and Burattini [34] (see also Figs. 3 and 6). Note that Frisch [12] (Fig. 8.6 therein) and Malecot [71] (Fig. 1.6 therein) also reported the same Modane data, but with a maximum value of $-\overline{(\delta u^*)^3}/r^*$ in excess of 4/5. As discussed below in the context of Fig. 1(c), this is most likely caused by an underestimation of $\bar{\epsilon}$; note that the magnitude of $\bar{\epsilon}$ reported by Malecot [71] (≈ 0.73 m^2/s^3) is about 23% smaller than that of Gagne *et al.* [46] (≈ 0.95 m^2/s^3). After renormalizing the distributions of $-\overline{(\delta u^*)^3}/r^*$

of Malecot [71] and Frisch [12] with $\bar{\epsilon} \approx 0.95 \text{ m}^2/\text{s}^3$, we found that they collapse reasonably well with that of Gagne *et al.* [46] [not shown in Fig. 1(a)]. The renormalized $\overline{(\delta u^*)^2}/r^{*2/3}$ distribution of Frisch [12] is shown in Figs. 4(a) and 6(a). Note that the Modane data were obtained in the return leg of the tunnel where the flow characteristics are not documented. They can at best be described as pseudogrid turbulence data. They are shown here since they have already been used extensively in the literature.

(iii) Included in Fig. 1(c) are the circular jet data ($\text{Re}_\lambda = 835$) of Anselmet *et al.* [50], which provided the first strong evidence for the so-called anomaly of the scaling exponents, i.e., the difference between ζ_n and $n/3$ continues to increase as n increases (beyond $n = 3$). For Anselmet *et al.* [50] (also circular jet data at $\text{Re}_\lambda = 966$), the maximum value of $-\overline{(\delta u^*)^3}/r^*$ exceeds 4/5. Lindborg [33] pointed out that this is incorrect since the second and third terms on the right-hand side of Eq. (2) should be negative if the Reynolds number is finite. The behavior is most likely caused by an underestimation of $\bar{\epsilon}$ due to the use of $\bar{\epsilon}_{iso}$ [$=15\nu\overline{(\partial u/\partial x)^2}$]. This is a problem with experimental data since, with rare exceptions (see, e.g., [72–74]), the full mean energy dissipation rate [$\equiv \frac{\nu}{2}\overline{(\frac{\partial u_i}{\partial x_j} + \frac{\partial u_j}{\partial x_i})^2}$ ($i, j = 1, 2, 3$)], only available for direct numerical simulation data, is estimated by its one-dimensional surrogate $\bar{\epsilon}_{iso}$ in measurements. Nevertheless, the absence of a plateau in Fig. 1 is unaffected by the actual value of $\bar{\epsilon}$ and hence by the manner in which $\bar{\epsilon}$ is estimated. The largest Re_λ ($=1840$) data on the axis of a circular water jet that have been published are those of Boffetta and Romano [75]. Distributions of $\overline{(\delta u^*)^3}$ are not shown in the paper but one can infer from the plotted variations (Fig. 3 of their paper) with r^* of $\overline{(\delta u)^2}$ and $\overline{(\delta u)^4}$ that Eq. (3) is unlikely to be satisfied.

(iv) We recall that SFPBT was first studied because it was expected that an IR would be possible at smaller values of Re_λ than in decaying flows, such as shearless grid turbulence. This expectation is fully consistent with the Navier-Stokes equation, as shown by Antonia and Burattini [34]. Several investigations have claimed to have established the 4/5 IR in a convincing manner in SFPBT. For example, Yeung *et al.* [58] claimed that their data at $\text{Re}_\lambda = 700$ exhibited a 4/5 plateau. Iyer *et al.* [56] claimed that Eq. (3) is satisfied to an accuracy of better than 5% at $\text{Re}_\lambda = 1300$, which corresponds to an IR of about one decade in extent. Their data have been reproduced in Fig. 1(e). It is clear that a 4/5 IR has not been attained even for $\text{Re}_\lambda = 1300$. All the data in Fig. 1(e) exhibit a convex curvature and, even at $\text{Re}_\lambda = 1300$, are at best tangential to the 4/5 line. Note that, at $\text{Re}_\lambda = 700$, the magnitude of $-\overline{(\delta u^*)^3}/r^*$ over the range $100 \lesssim r^* \lesssim 500$ exceeds 4/5. Yeung *et al.* [58] pointed out that, for their simulations, this magnitude is sensitive to the temporal variability of the volume-averaged $\bar{\epsilon}$ which, being driven by large scales, can vary by as much as 50% even in a period of statistical stationarity. This could explain why the magnitude of $-\overline{(\delta u^*)^3}/r^*$ is smaller at $\text{Re}_\lambda = 1300$ than that at $\text{Re}_\lambda = 1131$. As expected, the behavior of $-\overline{(\delta u^*)^3}/r^*$ in the dissipative range [Fig. 1(e)] seems immune to the influence of the large scales.

As discussed in the context of Eq. (2), only when the viscous and large-scale terms become negligible over a sufficiently large range of r^* can the IR be unequivocally established in decaying HIT. To illustrate this, we show in Fig. 3(a) distributions of $\overline{(\delta u^*)^3}/r^*$ at $\text{Re}_\lambda = 51, 89, 144, 200, 430, 2260, 10^4$, and 10^5 estimated from (2) with a parametrized form of $\overline{(\delta u^*)^2}$ in decaying HIT [34,39,76], viz.,

$$\overline{(\delta u^*)^2} = \frac{r^{*2}(1 + r^*/L^*)^{-2/3}}{15[1 + (r^*/r_c^*)^2]^{2/3}}, \tag{11}$$

where $r_c^* = (15C_{u2})^{3/4}$ (C_{u2} is the usually accepted value for the Kolmogorov constant, although the universality of this value has not yet been established rigorously) has been interpreted as a measure of the crossover between the dissipative and scaling ranges [77]. For isotropic turbulence, $L^* = C_\epsilon 15^{-3/4}\text{Re}_\lambda^{3/2}$. We stress that the parameters C_ϵ and C_{u2}, which feature in Eq. (11), can be adjusted in different flows (or different regions of the same flow) since Eq. (11) is mainly used to

provide an adequate fit to measurements of $\overline{(\delta u)^2}$ in a particular flow (or flow region). This allows us to extrapolate to values of Re_λ which cannot be achieved by measurement. The grid turbulence distributions in Fig. 3(a) were calculated using Eqs. (11) and (2), where I_u is given by (see, e.g., [32,78,79])

$$I_u(r) = \frac{3}{r^4} \int_0^r s^4 \left[U \frac{\partial \overline{(\delta u)^2}}{\partial x} \right] ds, \tag{12}$$

where U is the mean velocity in the x direction. For the axisymmetric jet, the distributions were calculated with I_u [80,81] given by

$$I_u = \frac{3}{r^4} \int_0^r s^4 \left[U \frac{\partial \overline{(\delta u)^2}}{\partial x} - 2[\overline{(\delta u)^2} - \overline{(\delta v)^2}] \frac{\partial U}{\partial x} \right] ds, \tag{13}$$

where v is the velocity fluctuation along the y direction. The corresponding local slope $LS_3(r^*)$ [$= d \log \overline{(\delta u^*)^3}/d \log r^*$], based on Eq. (11), at $Re_\lambda = 51, 89, 144, 200, 430, 2260, 10^4$, and 10^5 is shown in Fig. 3(b). Also shown in Fig. 3(a) are the grid turbulence data at $Re_\lambda = 51, 89, 144$, and 2260 [see also Fig. 1(a)] and circular jet data at $Re_\lambda = 200$ and 430 [see also Fig. 1(c)]. The agreement between curves and symbols in Fig. 3(a) is satisfactory, confirming the fit used to emulate the available data for $\overline{(\delta u^*)^2}$. No plateau can be observed in Fig. 3(a), even for $Re_\lambda = 10^5$, a value well beyond the reach of laboratory experiments and direct numerical simulations. The maximum value (0.795) at $Re_\lambda = 10^5$ is slightly below 4/5. The corresponding value of $LS_3(r^*)$ [Fig. 3(b)] appears to be close to 1, but in fact Fig. 3(b) shows that, if an exaggerated linear scale is used for the ordinate, the slope is equal to 1 only at one point ($r^* \approx 700$).

III. RESULTS FOR $\overline{(\delta u)^2}$

We show in Fig. 4 distributions of $\overline{(\delta u^*)^2}/(r^*)^{2/3}$ in nearly the same flows as in Fig. 1. Surprisingly, except for the Modane data shown by Frisch [12] at $Re_\lambda = 2260$ [we have renormalized these data with a more appropriate value of $\bar{\epsilon}$, as discussed in the context of Fig. 1(a)], we were unable to find data for $\overline{(\delta u^*)^2}$ in shearless grid turbulence for $Re_\lambda > 144$ in the literature. With regard to Fig. 4, the following points can be made.

(i) For sheared grid turbulence [Fig. 4(b)], there is a systematic increase with Re_λ as r^* increases. However, although the nondimensional shear parameter S^* ($= \frac{dU}{dy} \frac{\overline{u^2}}{\bar{\epsilon}_{iso}}$) is comparable ($\approx 5.0$–7.7) for all the data sets, the magnitudes of $\overline{(\delta u^*)^2}/(r^*)^{2/3}$ at $Re_\lambda = 875$ and 938 reported by Shen and Warhaft [69] are lower than those presented by Shen and Warhaft [49] and Ferchichi and Tavoularis [48] at smaller Re_λ ($= 170$–660). This may be due to a difference in initial conditions since an active grid was used by Shen and Warhaft [69] whereas a passive grid was used by Shen and Warhaft [49] and Ferchichi and Tavoularis [48]. Similarly, for SFPBT [Fig. 4(e)], different types of forcing may affect the behavior of $\overline{(\delta u^*)^2}/(r^*)^{2/3}$ differently. For example, the distribution for $Re_\lambda = 240$ reported by Yeung and Zhou [43] lies above that of McComb et al. [36] at a comparable Re_λ.

(ii) Except for the data of Ishihara et al. [22] which decrease systematically as Re_λ increases over the range $20 \lesssim r^* \lesssim 150$, the magnitude at a given r^*, say, $r^* = 100$, increases with Re_λ in all other box turbulence simulations [Fig. 4(e)].

(iii) There is reasonable collapse of the distributions in each flow in the range $r^* \lesssim 5$. Arguably, the collapse is most convincing when $\bar{\epsilon}$ is known accurately [e.g., Figs. 4(a) and 4(e)]. More importantly, the distributions in each flow increase systematically with Re_λ when r^* increases, implying (see [82]) that it would not be meaningful to assume a power-law behavior for $\overline{(\delta u^*)^2}$. This is further confirmed by the corresponding local slope [$LS_2(r^*) = d \log \overline{(\delta u^*)^2}/d \log r^*$] (Fig. 5) for the highest Re_λ in each of the flow types included in Fig. 4. The message from Figs. 4 and 5 is clear:
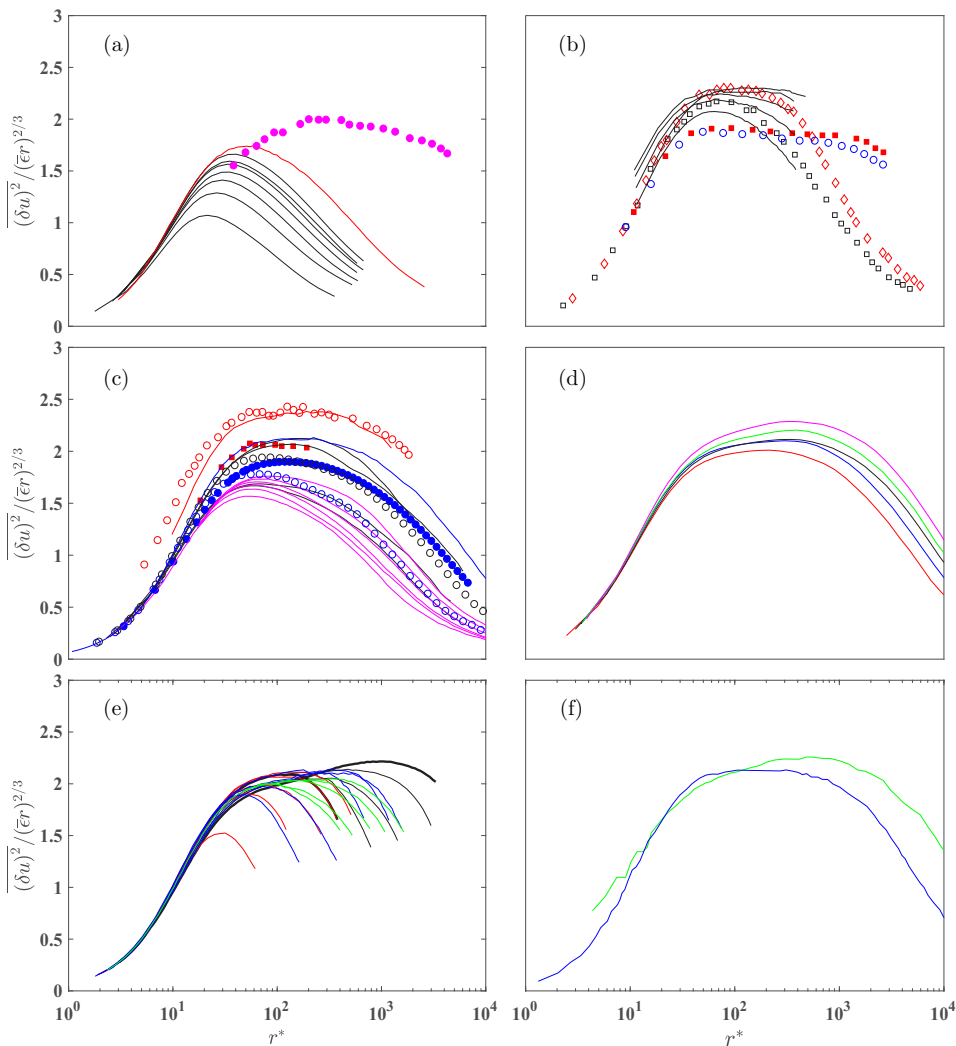
FIG. 4. (a) Distributions of $\overline{(\delta u^*)^2}/(r^*)^{2/3}$ in various flows. (a) Shearless grid turbulence: black curves, $Re_\lambda = 26$–99 [40]; red curve, $Re_\lambda = 144$ [71]; and ●, Modane data of Frisch [12] at $Re_\lambda = 2260$ (the distributions were renormalized with a more appropriate value of $\overline{\epsilon}$; see the text). (b) Sheared grid turbulence: black curves, $Re_\lambda = 170$–660 [48]; ○, $Re_\lambda = 875$ [69]; ■, $Re_\lambda = 938$ [69]; □, $Re_\lambda = 196$ [49]; and ◇, $Re_\lambda = 254$ [49]. (c) Along the axis in the far field of the circular jet: red curve, $Re_\lambda = 835$ [50]; ■, $Re_\lambda = 536$ [50]; ○, $Re_\lambda = 966$ [51]; black curves, $Re_\lambda = 235$–545 [52]; ●, $Re_\lambda = 485$ [41]; pink curves, $Re_\lambda = 122$–310 [53]; blue curve, $Re_\lambda = 695$ [71]; ○, $Re_\lambda = 200$ [54]; and ◯, $Re_\lambda = 430$ [54]. (d) Along the axis in the far field of the plane jet: $Re_\lambda = 550$–1067 [44]. (e) SFPBT: red curves, $Re_\lambda = 38$–240 [43]; green curves, $Re_\lambda = 177$–435 [36]; blue curves, $Re_\lambda = 70$–460 [42]; black curves, $Re_\lambda = 167$–1131 [22]. Note that thick lines are used for the distributions at the lowest and highest Re_λ. (f) Boundary layer at $Re_\lambda = 600$ (blue curve) and 1450 (green curve) [26].

There is no discernible plateau, i.e., $\overline{(\delta u)^2}$ does not exhibit a power-law variation. Interestingly, the local slope for $Re_\lambda = 966$ (circular jet) and 938 (sheared grid turbulence) appears to be close to 2/3 over a very small range of r^*; for the corresponding distributions in Fig. 2, LS_3 is not equal to 1. This leaves open the possibility that, for a given flow at a fixed initial condition, $\zeta_2 = 2/3$ may be
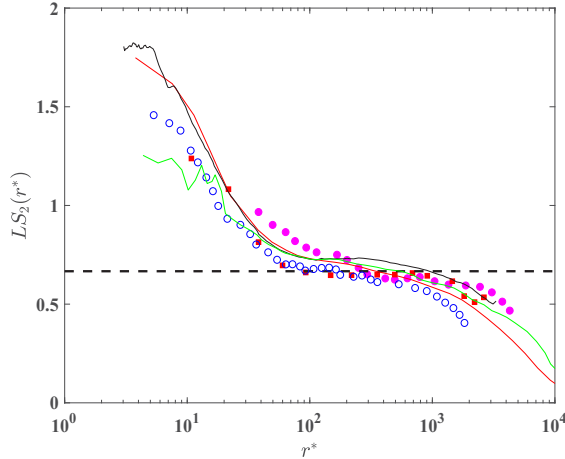
FIG. 5. Local slope $[\mathrm{LS}_2(r^*) = d \log \overline{(\delta u^*)^2}/d \log r^*]$ corresponding to the highest Re_λ in each plot of Fig. 4: ●, $\mathrm{Re}_\lambda = 2260$ [shearless grid turbulence; see Fig. 4(a)]; ■, $\mathrm{Re}_\lambda = 938$ [sheared grid turbulence; see Fig. 4(b)]; ○, $\mathrm{Re}_\lambda = 966$ [circular jet; see Fig. 4(c)]; red curve, $\mathrm{Re}_\lambda = 1067$ [plane jet; see Fig. 4(d)]; black curve, $\mathrm{Re}_\lambda = 1131$ [SFPBT; see Fig. 4(e)]; and green curve, $\mathrm{Re}_\lambda = 1450$ [boundary layer; see Fig. 4(f)]. The black dashed line corresponds to the value of 2/3.

achieved at a somewhat smaller Re_λ than $\zeta_3 = 1$. To further illustrate this, we show in Fig. 6(a) the distributions of $\overline{(\delta u^*)^2}/(r^*)^{2/3}$ at $\mathrm{Re}_\lambda = 59, 89, 144, 200, 430, 2260, 10^4$, and 10^5 calculated with Eq. (11) and the experimental data at $\mathrm{Re}_\lambda = 59, 89, 144, 200, 430$, and 2260. Although there is no clear plateau for $\mathrm{Re}_\lambda \leqslant 10^4$, the distribution [Fig. 6(b)] for $\mathrm{Re}_\lambda = 10^5$ shows a plateau slightly more than one decade in extent.

Equation (11) was tested against grid turbulence measurements by Antonia and Burattini [34] ($\mathrm{Re}_\lambda \lesssim 100$); it has been tested more thoroughly here against several data sets, obtained in different flows and in particular larger values of Re_λ. Figure 6(a) shows that the model-based curves are in reasonable agreement with both the grid turbulence and jet data. In Eq. (11), C_ϵ and C_{u2} were chosen to be 1.2 and 2.0 for grid turbulence and 1.4 and 2.0 for circular jet. For the $\mathrm{Re}_\lambda = 2260$ Modane data, the agreement is adequate for $r^* > 150$ but weaker for $r^* < 150$ due, most likely, to the increasing measurement difficulty as r^* decreases and Re_λ increases; this impairment is consistent with the displacement at small r^* of the Modane data for $\overline{(\delta u^*)^3}$ in Fig. 3(a).

Equation (11) was also tested extensively, for $\beta \equiv L^{*-1} = 0$ (i.e., over the dissipative range and most of the scaling range), by Antonia et al. [83] for different flows and by Stolovitzky et al. [84] in a turbulent boundary layer over a smooth wall. We should recall that Eq. (11), with $\beta = 0$, was first introduced by Batchelor [85] in the context of obtaining an analytical expression for the mean-square pressure gradient. Batchelor [85] assumed that $\overline{(\delta u^*)^2}$ depends only on r^*, i.e., it is a universal function which is quadratic ($=r^{*2}/15$) when $r^* \ll 1$ and tends to $C_{u2} r^{*2/3}$ when $r^* \gg 1$ as the Reynolds number approaches infinity. The inclusion of the term containing β does not affect the tendency toward $C_{u2} r^{*2/3}$ when $r^* \ll L$ (and $r^* \gg 1$). This term reflects how $\overline{(\delta u)^2}$ is influenced by the Reynolds number through the effect of the large scales. When r exceeds L, $\overline{(\delta u^*)^2}$ must, for a given Re_λ, approach a constant value, i.e., $2\overline{u^{*2}}$. Equation (11) satisfies this requirement. The asymptotic form of Eq. (11) in the IR, i.e., $C_{u2} r^{*2/3}$, is of course consistent with the result first obtained by Kolmogorov [1] via dimensional arguments; this approach is considerably bolstered by the fact that v_K and η have been shown [25,45] to be the appropriate similarity variables which satisfy the transport equation for $\overline{(\delta u)^2}$ over a range of scales for which the large-scale term can be neglected. As noted in Ref. [1], the 2/3 law is compatible with Eq. (3) if one assumes the skewness
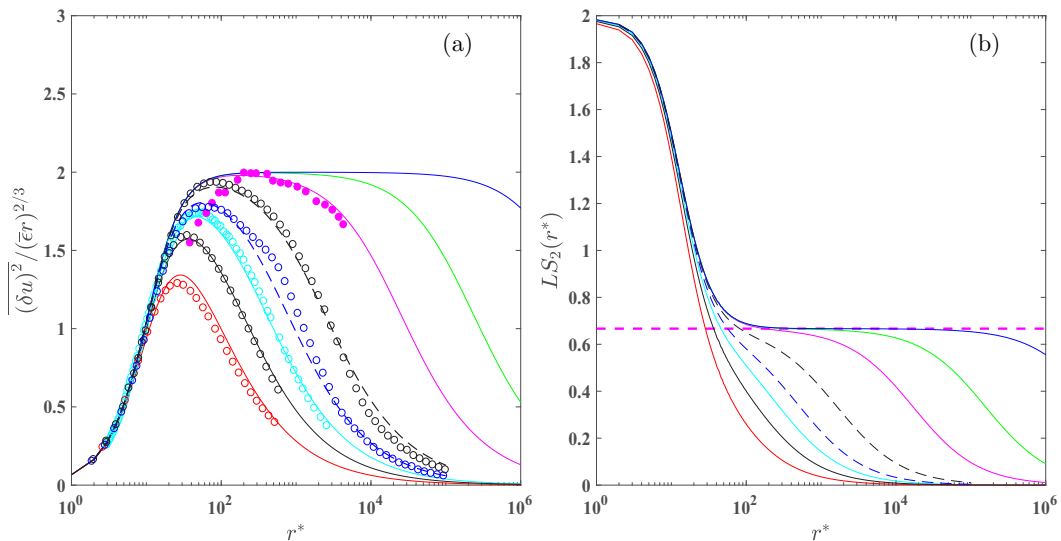
FIG. 6. (a) Distributions of $\overline{(\delta u)^2}/(\bar{\epsilon} r)^{2/3}$ based on Eq. (2) at $Re_\lambda = 51$ (red curve), $Re_\lambda = 89$ (black solid curve), $Re_\lambda = 144$ (cyan curve), $Re_\lambda = 200$ (blue dashed curve), $Re_\lambda = 430$ (black dashed curve), $Re_\lambda = 2260$ (pink curve), $Re_\lambda = 10^4$ (green curve), and $Re_\lambda = 10^5$ (blue solid curve). The symbols are the grid turbulence data [see Fig. 4(a)] at $Re_\lambda = 51$ (○), $Re_\lambda = 89$ (○), $Re_\lambda = 144$ (○), and $Re_\lambda = 2260$ (●). Also shown are the circular jet data [see Fig. 4(c)] at $Re_\lambda = 200$ (○) and $Re_\lambda = 430$ (○). Note that $C_\epsilon \approx 1.4$ is used for circular jet whereas $C_\epsilon \approx 1.2$ is used for grid turbulence; see the text. (b) Corresponding local slope [$LS_2(r^*) = d \log \overline{(\delta u^*)^2}/d \log r^*$] at $Re_\lambda = 51$ (red curve), $Re_\lambda = 89$ (black solid curve), $Re_\lambda = 144$ (cyan curve), $Re_\lambda = 200$ (blue dashed curve), $Re_\lambda = 430$ (black dashed curve), $Re_\lambda = 2260$ (pink curve), $Re_\lambda = 10^4$ (green curve), and $Re_\lambda = 10^5$ (blue curve). The dashed horizontal line corresponds to 2/3.

of δu to be constant in the IR. This is consistent with the assumption of scale invariance of δu across the IR [86]. Figures 3(a) and 6(a) indicate that the range over which self-similarity (or scale invariance) is applicable extends to larger values of r^* as Re_λ increases. The inference is that scale invariance will eventually be satisfied across the IR as $Re_\lambda \to \infty$, thus leading to the 2/3 law. If this scenario is correct, the possibility that $\overline{(\delta u^*)^2} \to r^{*2/3}$ as $Re_\lambda \to \infty$ cannot be discounted. What is important, in the context of this paper, is that Eq. (11) provides a satisfactory description of $\overline{(\delta u)^2}$ at small Reynolds numbers where the influence of the large scales cannot be ignored (see Fig. 6). This increases confidence in the extrapolation to values of Re_λ sufficiently large for the external scales to have a negligible effect on the IR.

In order to quantify, albeit approximately, the value of Re_λ required for an IR to be established, the range of r^* over which the distributions, based on Eq. (11), of $\overline{(\delta u^*)^2} r^{*-2/3}$ and $\overline{(\delta u^*)^3} r^{*-1}$ depart from 2 and 4/5, respectively, by no more than 2.5%, is identified in Fig. 7. It is clear that the IR is extended in size as Re_λ increases. Values of Re_λ of about 10^4 and 10^5 are required before one can claim a two-decade IR for $\overline{(\delta u)^2}$ and $\overline{(\delta u)^3}$, respectively. This is consistent with the implication, from Figs. 2 and 5, that for a given flow and fixed initial condition, $\zeta_2 = 2/3$ may be attained at a smaller Re_λ than $\zeta_3 = 1$. Similarly, it would not be unreasonable to expect that $\zeta_3 = 1$ will be attained at a smaller Re_λ than $\zeta_4 = 4/3$ and so on.

IV. CONCLUSION

The 4/5 law [Eq. (3)] is considered to be an exact result in turbulence. It is valid only when the large scales and viscosity cease to have an effect on the IR. Indeed, Eq. (3) was derived by
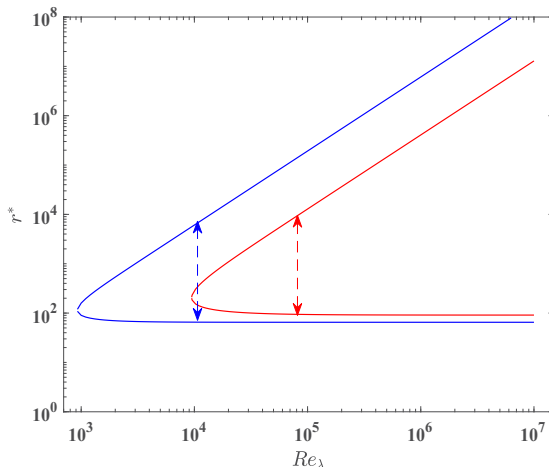
FIG. 7. Range of r^* over which $\overline{(\delta u^*)^2}r^{*-2/3}$ (blue line) and $\overline{(\delta u^*)^3}r^{*-1}$ (red line) depart from 2 and 4/5, respectively, by no more than 2.5%. The locations of the vertical arrows give an approximate indication of the values of Re_λ needed to attain an IR, of two decades in extent, for $\overline{(\delta u^*)^2}$ and $\overline{(\delta u^*)^3}$, respectively.

Kolmogorov [2] after neglecting the nonstationary term in Eq. (2) by assuming that the Reynolds number is infinitely large. Equation (3) was derived in K41 and assumed in K62. We have carried out a relatively extensive review of results available in the literature for $\overline{(\delta u)^3}$ and also $\overline{(\delta u)^2}$. The main conclusion that can be drawn from this review is that the maximum value of Re_λ that has been achieved in the laboratory is insufficient for these two quantities to display a power-law behavior. Correspondingly, there is no evidence that an IR has been established. It is nonetheless inevitable that Eq. (3) will be validated when the nonstationary term I_u in Eq. (2) is no longer important. The use of Eq. (3) together with an empirical model for $\overline{(\delta u)^2}$ confirms the earlier result of Antonia and Burattini [34], viz., Re_λ needs to exceed 10^5 before one can claim an IR for $\overline{(\delta u)^2}$ of about two decades in extent. Although the model for $\overline{(\delta u)^2}$ asymptotes towards $r^{2/3}$ at very large Re_λ, it is in reasonable accord with the measurements of $\overline{(\delta u)^2}$ and $\overline{(\delta u)^3}$ for values of Re_λ up to about 10^3, thus providing confidence when extrapolating the model-based results to larger values of Re_λ.

The results, based on Eqs. (2) and (11), indicate that the IR for $\overline{(\delta u)^2}$ is approached at a slightly faster rate than that for $\overline{(\delta u)^3}$ (Figs. 2, 5, and 7); this is not surprising given the close link that exists, through Eq. (2), between lower- and higher-order moments of δu and the expectation that lower-order moments should reach their asymptotic states at lower Reynolds numbers than higher-order moments. Since there is a hierarchy of equations (see, e.g., [87]) linking lower- and higher-order moments of δu, all derived from the Navier-Stokes equation, one expects that the value of Re_λ required for a moment of order n to reach its asymptotic state will increase as n increases. This raises a major concern with regard to the distribution of ζ_n vs n (see, e.g., [12,13,16,50]) that is generally assumed to be independent of Re_λ and has been more or less reproduced by several intermittency models (see, e.g., [13]). The departure, referred to as anomalous scaling, of this distribution from the K41 prediction $\zeta_n = n/3$ [Eq. (4)] has been attributed to the effect of intermittency. This departure needs to be reappraised critically in light of Figs. 2, 5 and 7.

The reasonably good collapse of $\overline{(\delta u^*)^3}$ [Figs. 1(d)–1(f)] and $\overline{(\delta u^*)^2}$ [Figs. 4(a), 4(d), and 4(e)] at small r^* supports the first similarity hypothesis of K41 with the important qualification that Re_λ does not need to be very large. The extent of the similarity (or scale invariance) is observed to increase as Re_λ increases; the possibility that the second hypothesis of K41 may be verified at very large Re_λ cannot be excluded, especially if we are guided by the extrapolation (Fig. 7) based on

Eqs. (2) and (11). This, together with the recent observations that quantities like the skewness and flatness factor of $\partial u/\partial x$ are bounded [44,61,65–68] at sufficiently large Re_λ, strongly supports the notion that, in the context of locally HIT turbulence, K41 cannot be ruled out when $Re_\lambda \to \infty$.

As underlined by McComb [19], K62 is predicated on the idea that the effect of the larger scales is experienced at all small scales. We pointed out in the Introduction that this idea is inconsistent with the retention of the 4/5 law or Eq. (3). The validity of Eq. (3) requires that the large scales cannot affect the IR and, *a fortiori*, the dissipative range; Eq. (3) follows from Eq. (2) once the effect of the large scales (or nonstationarity) is discounted and the influence of viscosity is neglected. Nevertheless, all intermittency models have to date been tested in situations described by Eq. (2) with the caveat that the nonstationarity term assumes different forms in different flows. In the context of dissipative range scales, these models are best interpreted as attempts to describe the effect of the large scales or, equivalently, the effect of Re_λ on small-scale characteristics. In the context of IR scales, the models have reproduced the apparently anomalous behavior of ζ_n, the anomaly or departure from $n/3$ (or K41) increasing with n, with the notable exception of ζ_3, which has been assumed to be equal to 1. The present results, like those of McComb *et al.* [36], indicate that the anomalous values of ζ_2 are very likely associated with the FRN effect; Qian [29] was in fact first to draw attention to this. More importantly, the present results also emphasize that ζ_3 should never have been assumed to be equal 1; the latter value can only be reached at extremely large Reynolds numbers. The anomalous behavior of ζ_2 and ζ_3 when Re_λ is finite is fully consistent with Eq. (2). A bigger challenge will be to show that the apparent anomaly of ζ_n for $n > 3$ can be reconciled with the appropriate exact equations relating $\overline{(\delta u)^n}$ to $\overline{(\delta u)^{n+1}}$.

[1] A. N. Kolmogorov, The local structure of turbulence in incompressible viscous fluid for very large Reynolds number, Dokl. Akad. Nauk SSSR **30**, 299 (1941); see also Proc. R. Soc. London Ser. A **434**, 9 (1991).

[2] A. N. Kolmogorov, Dissipation of energy in the locally isotropic turbulence, Dokl. Akad. Nauk SSSR **32**, 16 (1941); see also Proc. R. Soc. London Ser. A **434**, 15 (1991).

[3] T. von Kármán and L. Howarth, On the statistical theory of isotropic turbulence, Proc. R. Soc. London Ser. A **164**, 192 (1938).

[4] P. A. Davidson, Y. Kaneda, K. Moffatt, and K. R. Sreenivasan, *A Voyage through Turbulence* (Cambridge University Press, Cambridge, 2011).

[5] G. K. Batchelor, Kolmogoroff's theory of locally isotropic turbulence, Proc. Cambridge Philos. Soc. **43**, 533 (1947).

[6] H. L. Grant, R. W. Stewart, and A. Moilliet, Turbulence spectra from a tidal channel, J. Fluid Mech. **12**, 241 (1962).

[7] A. N. Kolmogorov, A refinement of previous hypotheses concerning the local structure of turbulence in a viscous incompressible fluid at high Reynolds number, J. Fluid Mech. **13**, 82 (1962).

[8] A. M. Oboukhov, Some specific features of atmospheric turbulence, J. Fluid Mech. **13**, 77 (1962).

[9] C. H. Gibson, G. R. Stegen, and R. B. Williams, Statistics of the fine structure of turbulent velocity and temperature fields at high Reynolds number, J. Fluid Mech. **41**, 153 (1970).

[10] J. C. Wyngaard and H. Tennekes, Measurements of the small-scale structure of turbulence at moderate Reynolds numbers, Phys. Fluids **13**, 1962 (1970).

[11] C. W. Van Atta and R. A. Antonia, Reynolds number dependence of skewness and flatness factors of turbulent velocity derivatives, Phys. Fluids **23**, 252 (1980).

[12] U. Frisch, *Turbulence: The Legacy of A. N. Kolmogorov* (Cambridge University Press, Cambridge, 1995).

[13] K. Sreenivasan and R. A. Antonia, The phenomenology of small-scale turbulence, Annu. Rev. Fluid Mech. **29**, 435 (1997).

[14] A. S. Monin and A. M. Yaglom, *Statistical Fluid Dynamics* (MIT Press, Cambridge, 2007), Vol. 2.

[15] A. M. Yaglom, in *Advances in Turbulence X, Proceedings of the Tenth European Turbulence Conference, Trondheim, 2004*, edited by H. I. Andersson and P. Å. Krogstad (CIMNE, Barcelona, 2004), pp. 443–448.

[16] F. Anselmet, R. A. Antonia, and L. Danaila, Turbulent flows and intermittency in laboratory experiments, Planet. Space Sci. **49**, 1177 (2001).

[17] G. Boffetta, A. Mazzino, and A. Vulpiani, Twenty-five years of multifractals in fully developed turbulence: a tribute to Giovanni Paladin, J. Phys. A: Math. Theor. **41**, 363001 (2008).

[18] P. G. Saffman, in *Structure and Mechanisms of Turbulence II*, edited by H. Fielder, Lecture Notes in Physics Vol. 76 (Springer, Berlin, 1978), pp. 273–306.

[19] W. D. McComb, *Homogeneous, Isotropic Turbulence, Phenomenology, Renormalization and Statistical Closures* (Oxford University Press, Oxford, 2014).

[20] K. R. Sreenivasan, On the scaling of the turbulence energy dissipation rate, Phys. Fluids **27**, 1048 (1984).

[21] P. Burattini, P. Lavoie, and R. Antonia, On the normalized turbulent energy dissipation rate, Phys. Fluids **17**, 98103 (2005).

[22] T. Ishihara, T. Gotoh, and Y. Kaneda, Study of high-Reynolds number isotropic turbulence by direct numerical simulation, Annu. Rev. Fluid Mech. **41**, 165 (2009).

[23] J. C. Vassilicos, Dissipation in turbulent flows, Annu. Rev. Fluid Mech. **47**, 95 (2015).

[24] W. D. McComb, A. Berera, S. R. Yoffe, and M. F. Linkmann, Energy transfer and dissipation in forced isotropic turbulence, Phys. Rev. E **91**, 043013 (2015).

[25] R. A. Antonia, L. Djenidi, and L. Danaila, Collapse of the turbulent dissipation range on Kolmogorov scales, Phys. Fluids **26**, 045105 (2014).

[26] S. G. Saddoughi and S. V. Veeravalli, Local isotropy of turbulent boundary layers at high Reynolds number, J. Fluid Mech. **268**, 333 (1994).

[27] K. R. Sreenivasan, On the universality of the Kolmogorov constant, Phys. Fluids **7**, 2778 (1995).

[28] T. von Kármán and C. C. Lin, On the concept of similiarity in the theory of isotropic turbulence, Rev. Mod. Phys. **21**, 516 (1949).

[29] J. Qian, Inertial range and the finite Reynolds number effect of turbulence, Phys. Rev. E **55**, 337 (1997).

[30] J. Qian, Slow decay of the finite Reynolds number effect of turbulence, Phys. Rev. E **60**, 3409 (1999).

[31] J. Qian, Normal and anomalous scaling of turbulence, Phys. Rev. E **58**, 7325 (1998).

[32] L. Danaila, F. Anselmet, T. Zhou, and R. A. Antonia, A generalization of Yaglom's equation which accounts for the large-scale forcing in heated decaying turbulence, J. Fluid Mech. **391**, 359 (1999).

[33] E. Lindborg, Correction to the four-fifths law due to variations of the dissipation, Phys. Fluids **11**, 510 (1999).

[34] R. A. Antonia and P. Burattini, Approach to the 4/5 law in homogeneous isotropic turbulence, J. Fluid Mech. **550**, 175 (2006).

[35] J. Tchoufag, P. Sagaut, and C. Cambon, Spectral approach to finite Reynolds number effects on Kolmogorov's 4/5 law in isotropic turbulence, Phys. Fluids **24**, 015107 (2012).

[36] W. D. McComb, S. R. Yoffe, M. F. Linkmann, and A. Berera, Spectral analysis of structure functions and their scaling exponents in forced isotropic turbulence, Phys. Rev. E **90**, 053010 (2014).

[37] J. Boschung, M. Gauding, F. Hennig, D. Denker, and H. Pitsch, Finite Reynolds number corrections of the 4/5 law for decaying turbulence, Phys. Rev. Fluids **1**, 064403 (2016).

[38] R. R. Mills, Jr., A. L. Kistler, V. O'Brien, and S. Corrsin, Turbulence and temperature fluctuations behind a heated grid, NACA Report No. 4288, 1958.

[39] R. A. Antonia, R. J. Smalley, T. Zhou, F. Anselmet, and L. Danaila, Similarity of energy structure functions in decaying homogeneous isotropic turbulence, J. Fluid Mech. **487**, 245 (2003).

[40] T. Zhou and R. A. Antonia, Reynolds number dependence of the small-scale structure of grid turbulence, J. Fluid Mech. **406**, 81 (2000).

[41] B. R. Pearson and R. A. Antonia, Reynolds-number dependence of turbulent velocity and pressure increments, J. Fluid Mech. **444**, 343 (2001).

[42] T. Gotoh, D. Fukayama, and T. Nakano, Velocity field statistics in homogeneous steady turbulence obtained using a high-resolution direct numerical simulation, Phys. Fluids **14**, 1065 (2002).

[43] P. K. Yeung and Y. Zhou, Universality of the Kolmogorov constant in numerical simulations of turbulence, Phys. Rev. E **56**, 1746 (1997).

[44] S. L. Tang, R. A. Antonia, L. Djenidi, L. Danaila, and Y. Zhou, Finite Reynolds number effect on the scaling range behavior of turbulent longitudinal velocity structure functions, J. Fluid Mech. **820**, 341 (2017).

[45] L. Djenidi, R. A. Antonia, and L. Danaila, Self-preservation relation to the Kolmogorov similarity hypotheses, Phys. Rev. Fluids **2**, 054606 (2017).

[46] Y. Gagne, B. Castaing, C. Baudet, and Y. Malecot, Reynolds dependence of third-order velocity structure functions, Phys. Fluids **16**, 482 (2004).

[47] L. Mydlarski and Z. Warhaft, On the onset of high- Reynolds-number grid-generated wind tunnel turbulence, J. Fluid Mech. **320**, 331 (1996).

[48] M. Ferchichi and S. Tavoularis, Reynolds number effects on the fine structure of uniformly sheared turbulence, Phys. Fluids **12**, 2942 (2000).

[49] X. Shen and Z. Warhaft, Longitudinal and transverse structure functions in sheared and unsheared wind-tunnel turbulence, Phys. Fluids **14**, 370 (2002).

[50] F. Anselmet, Y. Gagne, E. J. Hopfinger, and R. A. Antonia, Higher-order velocity structure functions in turbulent shear flows, J. Fluid Mech. **140**, 63 (1984).

[51] R. A. Antonia, B. R. Satyaprakash, and A. J. Chambers, Reynolds number dependence of velocity structure functions in turbulent shear flows, Phys. Fluids **25**, 29 (1982).

[52] G. Xu, R. A. Antonia, and S. Rajagopalan, Sweeping decorrelation hypothesis in a turbulent round jet, Fluid Dyn. Res. **28**, 311 (2001).

[53] H. Sadeghi, P. Lavoie, and A. Pollard, The effect of Reynolds number on the scaling range along the centreline of a round turbulent jet, J. Turbul. **15**, 335 (2014).

[54] L. Djenidi, R. A. Antonia, N. Lefeuvre, and J. Lemay, Complete self-preservation on the axis of a turbulent round jet, J. Fluid Mech. **790**, 57 (2016).

[55] T. Gotoh and T. Watanabe, Power and Nonpower Laws of Passive Scalar Moments Convected by Isotropic Turbulence, Phys. Rev. Lett. **115**, 114502 (2015).

[56] K. P. Iyer, K. R. Sreenivasan, and P. K. Yeung, Reynolds number scaling of velocity increments in isotropic turbulence, Phys. Rev. E **95**, 021101(R) (2017).

[57] K. P. Iyer, K. R. Sreenivasan, and P. K. Yeung, Refined similarity hypothesis using three-dimensional local averages, Phys. Rev. E **92**, 063024 (2015).

[58] P. K. Yeung, D. A. Donzis, and K. R. Sreenivasan, High-Reynolds-number simulation of turbulent mixing, Phys. Fluids **17**, 081703 (2005).

[59] F. Moisy, P. Tabeling, and H. Willaime, Kolmogorov Equation in a Fully Developed Turbulence Experiment, Phys. Rev. Lett. **82**, 3994 (1999).

[60] L. Djenidi, R. A. Antonia, M. K. Talluru, and H. Abe, Skewness and flatness factors of the longitudinal velocity derivative in wall-bounded flows, Phys. Rev. Fluids **2**, 064608 (2017).

[61] S. L. Tang, R. A. Antonia, L. Djenidi, L. Danaila, and Y. Zhou, Reappraisal of the velocity derivative flatness factor in various turbulent flows, J. Fluid Mech. **847**, 244 (2018).

[62] K. R. Sreenivasan and B. Dhruva, Is there scaling in high-Reynolds-number turbulence? Prog. Theor. Phys. Suppl. **130**, 103 (1998).

[63] M. Kholmyansky, A Tsinober, and S. Yorish, Velocity derivatives in the atmospheric surface layer at $Re_\lambda = 10^4$, Phys. Fluids **13**, 311 (2001).

[64] M. Kholmyansky and A. Tsinober, Kolmogorov 4/5 law, nonlocality, and sweeping decorrelation hypothesis, Phys. Fluids **20**, 041704 (2008).

[65] R. A. Antonia, S. L. Tang, L. Djenidi, and L. Danaila, Boundedness of the velocity derivative skewness in various turbulent flows, J. Fluid Mech. **781**, 727 (2015).

[66] S. L. Tang, R. A. Antonia, L. Djenidi, H. Abe, T. Zhou., L. Danaila, and Y. Zhou, Transport equation for the meant turbulent energy dissipation rate on the centreline of a fully developed channel flow, J. Fluid Mech. **777**, 151 (2015).

[67] S. L. Tang, R. A. Antonia, L. Djenidi, and Y. Zhou, Transport equation for the meant turbulent energy dissipation rate in the far-wake of a circular cylinder, J. Fluid Mech. **784**, 109 (2015).

[68] R. A. Antonia, L. Djenidi, L. Danaila, and S. L. Tang, Small scale turbulence and the finite Reynolds number effect, Phys. Fluids **29**, 020715 (2017).

[69] X. Shen and Z. Warhaft, The anisotropy of the small scale structure in high Reynolds number ($R_\lambda \sim 1000$) turbulent shear flow, Phys. Fluids **12**, 2976 (2000).

[70] H. Kahalerras, Y. Malécot, and Y. Gagne, Intermittency and Reynolds number, Phys. Fluids **10**, 910 (1998).

[71] Y. Malecot, Intermittence en turbulence 3D: Statistiques de la vitesse et de la vorticité, Ph.D. thesis, University of Grenoble, 1998.

[72] L. W. Browne, R. A. Antonia, and D. A. Shah, Turbulent energy dissipation in a wake, J. Fluid Mech. **179**, 307 (1987).

[73] R. A. Antonia, T. Zhou, and Y. Zhu, Three-component vorticity measurements in a turbulent grid flow, J. Fluid Mech. **374**, 29 (1998).

[74] G. Gulitski, M. Kholmyansky, W. Kinzelbach, B. Luthi, A. Tsinober, and S. Yorish, Velocity and temperature derivatives in high-Reynolds-number turbulent flows in the atmospheric surface layer. Part 1. Facilities, methods and some general results, J. Fluid Mech. **589**, 57 (2007).

[75] G. Boffetta and G. P. Romano, Structure functions and energy dissipation dependence on Reynolds number, Phys. Fluids **14**, 3453 (2002).

[76] S. Kurien and K. R. Sreenivasan, Anisotropic scaling contributions to high-order structure functions in high-Reynolds-number turbulence, Phys. Rev. E **62**, 2206 (2000).

[77] S. Grossmann and D. Lohse, Scale resolved intermittency in turbulence, Phys. Fluids **6**, 611 (1994).

[78] R. A. Antonia, T. Zhou, L. Danaila, and F. Anselmet, Streamwise inhomogeneity of decaying grid turbulence, Phys. Fluids **12**, 3086 (2000).

[79] L. Danaila, F. Anselmet, and R. A. Antonia, An overview of the effect of large-scale inhomogeneities on small-scale turbulence, Phys. Fluids **14**, 2475 (2002).

[80] P. Burattini, R. A. Antonia, and L. Danaila, Similarity in the far field of a turbulent round jet, Phys. Fluids **17**, 025101 (2005).

[81] F. Thiesset, R. A. Antonia, and L. Djenidi, Consequences of self-preservation on the axis of a turbulent round jet, J. Fluid Mech. **748**, R2 (2014).

[82] L. Djenidi, R. A. Antonia, and S. L. Tang, Scale invariance in finite Reynolds number homogeneous isotropic turbulence, J. Fluid Mech. **864**, 244 (2019).

[83] R. A. Antonia, B. R. Pearson, and T. Zhou, Reynolds number dependence of second-order velocity structure functions, Phys. Fluids **12**, 3000 (2000).

[84] G. Stolovitzky, K. R. Sreenivasan, and A. Juneja, Scaling functions and scaling exponents in turbulence, Phys. Rev. E **48**, R3217 (1993).

[85] G. K. Batchelor, Pressure fluctuation in isotropic turbulence, Proc. Cambridge Philos. Soc. **47**, 359 (1951).

[86] P. Davidson, *Turbulence: An Introduction for Scientists and Engineers* (Oxford University Press, Oxford, 2004).

[87] R. J. Hill, Equations relating structure functions of all orders, J. Fluid Mech. **434**, 379 (2001).